Supplement of Geosci. Model Dev., 16, 5847–5863, 2023
https://doi.org/10.5194/gmd-16-5847-2023-supplement

Geoscientific Model Development
Open Access

Supplement of

Representing the impact of *Rhizophora* mangroves on flow in a hydrodynamic model (COAWST_rh v1.0): the importance of three-dimensional root system structures

Masaya Yoshikai et al.

Correspondence to: Masaya Yoshikai (yoshikai.masaya@gmail.com)

Supporting Information

S1. Vegetation module implemented by Beudin et al. (2017)

As in the main text, we describe the equations in the two-dimensional form (*x*-*z* plane; zero velocity in *y*-direction) for convenience, while the equations implemented in ROM are three-dimensional; see Beudin et al. (2017) for the complete equations. The vegetation module implemented by Beudin et al. (2017) is for seagrasses/marshes that were represented by the cylinder drag model. They implemented the vegetation impacts not only on flows but also on wave damping. They also included additional functions of leaf bending considering the flexibility of submerged vegetations. Here we only describe the equations for impacts of rigid vegetation (no bending) on flow; these equations were used for comparison with the newly implemented drag and turbulence model for *Rhizophora* mangrove forests.

The drag by vegetation is calculated using the quadratic drag law as

$$F_{veg}(z) = \frac{1}{2} C_D n_v b_v u(z)^2 \quad \text{(S1)}$$

where F_{veg} is the spatially-averaged vegetation drag (m s^{-2}), z is the height from bed (m), C_D is the drag coefficient, n_v is the number of plants (stems or leaves) per unit area (m^{-2}), b_v is the stem or leaf width (m), and u is the flow velocity (m s^{-1}).

The production of turbulence kinetic energy (TKE) by vegetation drag is expressed as

$$P_w = F_{veg} u \quad \text{(S2)}$$

where P_w is the production of TKE by vegetation-generated wakes (m^2 s^{-3}). The dissipation rate of wakes is expressed as

$$D_w = c_2 \frac{P_w}{\tau_{eff}} = c_2 \frac{P_w}{min(\tau_{free}, \tau_{veg})} \quad \text{(S3)}$$

where D_w is the wake dissipation rate (m^2 s^{-4}), c_2 (1.92) is the constant of the k–ε model, and τ_{eff} (s) are the effective time-scale of wakes, which takes the minimum of time-scale of free turbulence (τ_{free}) and time-scale regulated by spaces between the nearest-neighbor plants (τ_{veg}). These are described as

$$\tau_{free} = \frac{k}{\varepsilon} \quad \text{(S4a)}$$

$$\tau_{veg} = \left(\frac{L^2}{c_w{}^2 P_w}\right)^{1/3} = \left(\frac{s^2}{c_w{}^2 P_w}\right)^{1/3} \quad \text{(S4b)}$$

where k is the TKE (m^2 s^{-2}), ε is the turbulent dissipation (m^2 s^{-3}), c_w is the model constant, which was set as 0.09 in Beudin et al. (2017), and L (m) is the length-scale of wakes, which was set as the mean spacing of nearest-neighbor plants (s) in Beudin et al. (2017) where s is calculated from the density, width, and thickness of stem/leaf.

S2. Minor modifications of k–ε model introduced by Beudin et al. (2017)

In Beudin et al. (2017), the time-scale of wakes (τ_{eff}) was defined by the minimum of τ_{free} and τ_{veg} as described in Eq. (S3) in Sect. S1. However, we noticed the minimum function used for τ_{eff} yields complicated results. This may be because of the interactive feedback between τ_{free} and τ_{veg}, such that a case of $\tau_{eff} = \tau_{veg}$ in Eq. (S3) at one moment affects τ_{free} at the next moment through the equations for k (Eq. 2) and ε (Eq. 3); these in turn will affect τ_{eff} in Eq. (S3). As a result, the original model by Beudin et al. (2017) predicted TKE significantly smaller than the model predictions using the time-scale set as either of τ_{free} and τ_{veg}, which are difficult to interpret (results not shown). This minimum function for the time-scale of wake turbulence has not been well supported by previous theoretical and experimental works. As such, we avoided the use of the minimum function for τ_{eff} in our analysis.

The use of τ_{free} for τ_{eff} corresponds to the time-scale used such as in López and García (2001), Defina and Bixio (2005), and Baptist et al. (2007). However, King et al. (2012) and Liu et al. (2017) found that the use of τ_{veg} for τ_{eff}, which explicitly specifies the length-scale of wakes (L in Eq. S4b), would produce much better results than the use of τ_{free} for τ_{eff}.

For τ_{veg}, the use of s for the length-scale, L, in Eq. (S4b) inherently assumes the conditions $s < d$, where d is the cylinder diameter, which is equal to b_v for the seagrasses/marshes, where otherwise d should be applied for L (Tanino and Nepf, 2008; Nepf, 2012). In our analysis performed in the main text, the cylinder approximations (Fig. 3) did not satisfy the conditions $s < d$, thus the d (= b_v) would be appropriate for L.

Based on these, we modified Eqs. (S3–4) as

$$D_w = c_2 \frac{P_w}{\tau_{veg}} \quad \text{(S5)}$$

$$\tau_{veg} = \left(\frac{L^2}{{c_w}^2 P_w}\right)^{1/3} = \left(\frac{{b_v}^2}{{c_w}^2 P_w}\right)^{1/3} \quad \text{(S6)}$$

These modified equations were used for the model analysis using the cylinder array approximations in the main text.

S3. *Rhizophora* root model

The vertical profile of root projected area density (a_{root}) was computed using the empirical model for *Rhizophora* root structures (*Rh*-root model) proposed by Yoshikai et al. (2021); the procedure is summarized below.

The model was designed to predict the structure of the individual root system. It predicts the vertical profile of the number of roots of a tree using two parameters–*S* (scaling factor) and HR_{max} (maximum root height). The *S* and HR_{max} are strongly related to tree size represented by the stem diameter measured at 1.3-m height (D_{stem}). The k^{th} highest root in a root system can be then expressed as

$$HR_k = HR_{max}S^{(k-1)} \geq HR_{min} \tag{S7a}$$

$$S = 1 - \beta_S {D_{stem,i}}^{\alpha_S} \tag{S7b}$$

$$HR_{max} = \alpha_{HR}D_{stem,i} + \beta_{HR} \tag{S7c}$$

where HR_{min} in Eq. (S7a) is a model parameter (critical root height) that limits the minimum root height of a tree, $D_{stem,i}$ is the stem diameter (m) where the subscript "*i*" represents tree index, and α_S, β_S, α_{HR}, β_{HR} are the scaling parameters for *S* and HR_{max}, respectively. The α_S, β_S, α_{HR}, β_{HR} are considered site- and species-specific parameters, thus the values need to be derived through a field survey. See Yoshikai et al. (2021) or (2022a) for the procedure to obtain these parameter values in the field with reduced workload. The value of HR_{min} also needs to be determined for a site through a field survey.

From Eq. (S7), the heights of all roots of a tree can be predicted. Yoshikai et al. (2022a) suggested that the individual roots can be approximated as a linear shape to estimate the projected area of roots. The linear shape of a root projected from the direction along the *x*-axis can be expressed as

$$z = (tan\theta_l)\left(\frac{y}{cos\psi}\right) + HR \qquad \text{where } 0 < z < HR \tag{S8}$$

where *y* and *z* represent the horizontal and vertical coordinate of a point, where $y = 0$ at the location where a root emerges from the stem or another root and $z = 0$ at the ground, *HR* is the height of a root (m), θ_l is the angle of the approximated linear shape relative to the horizontal axis, and ψ is the azimuth root angle around the *z*-axis relative to the *x*-axis. The value of θ_l was empirically determined in Yoshikai et al. (2022a). The projected area of a root can be calculated by multiplying the root length provided by Eq. (S8) and the mean root diameter ($D_{root,ave}$). Then, by summing up the projected areas of all the roots per vertical height interval, dz (0.05 m in this study), the vertical profile of root projected area per dz of a tree "i" ($A_{root,i}(z)$ (m^2)) can be calculated. Here, because the root azimuth angle in Eq. (8), ψ, is unknown, Yoshikai et al. (2022a) employed random numbers to ψ and estimated $A_{root,i}$ from the ensemble approach. Based on the ensemble computations, we found that the $A_{root,i}$ computed using random numbers for ψ is approximately 80 % of the $A_{root,i}$ computed using the zero value for ψ for all the roots, which is referred to as $A_{root0,i}$ below. Hence, we calculated the $A_{root,i}$ as

$$A_{root,i}(z) = 0.8 \times A_{root0,i}(z) \quad \text{(S9)}$$

where the multiplication by 0.8 represents the effects of random azimuth angle on the projected area. This approach (Eq. S9) does not require the ensemble approach to estimate $A_{root,i}$, which is convenient for implementation to the numerical model.

S4. Tree census data

We used tree census data collected from three sites–two from Bakhawan Ecopark, Aklan, Philippines (11° 43' N, 122° 23' E; Suwa et al., unpublished data), and one from Fukido River mangrove forest, Ishigaki, Japan (24° 20' N, 124° 15' E; Suwa et al., 2021)–to investigate the validity of the proposed parameterization of tree size variations (see Section 2.1.3). We refer to the two sites of Bakhawan Ecopark as Bak1 and Bak2, respectively, and Fukido River mangrove forest as Fuk.

The sites Bak1 and Bak2 are 30-year-old and 17-year-old planted stands, respectively, of *Rhizophora apiculata*; Bak2 includes the site where the vegetation and hydrodynamic data were collected by Yoshikai et al. (2022a), which were used for model evaluation in this study. The site Fuk is a natural mangrove forest vegetated by *Rhizophora stylosa* and *Buruguiera gymnorrhiza*. Along with the soil salinity gradient, a notable change in the forest structural variables (stem diameter, tree height, species composition) was observed at this forest (Yoshikai et al., 2022b). As described in Suwa et al. (2021), a 7-m radius circular plot was established and the stem diameter at 1.3-m height (D_{stem}) was measured for all the trees. The number of plots for the tree census is 6 for Bak1, 6 for Bak2, and 15 for Fuk, respectively. We did not use the data of 10 plots out of a total of 24 plots in Fuk collected in Suwa et al. (2021) because of the absence of *R. stylosa* trees.

The root structures of *R. apiculata* and *R. stylosa* at these three sites were investigated in Yoshikai et al. (2021) and the values of the *Rh*-root model parameters were derived (Table S1). These parameter values were used for the computation of the vertical profile of root projected area per dz of a tree, $A_{root,i}(z)$, for each site using the Rh-root model; these are shown in Fig. 2.

Table S1. *Rhizophora* root model parameters for three tree census sites.

Parameter	Bak1	Bak2	Fuk
Scaling parameter for S (α_S)	–0.91	–2.04	–1.76
Scaling parameter for S (β_S)	$10^{-2.00}$	$10^{-3.59}$	$10^{-3.18}$
Scaling parameter for S (α_{HR})	2.06	15.38	2.71
Scaling parameter for S (β_{HR})	0.82	0.08	0.50
Critical root height (HR_{min}, m)	0.01[a]	0.01	0.01[a]
Root angle of approximated linear root shape (θ_l, degree)	–34.5[a]	–34.5	–41.9
Mean root diameter ($D_{root,ave}$, m)	0.03[a]	0.03	0.03

[a] Value determined for Bak2 was used.

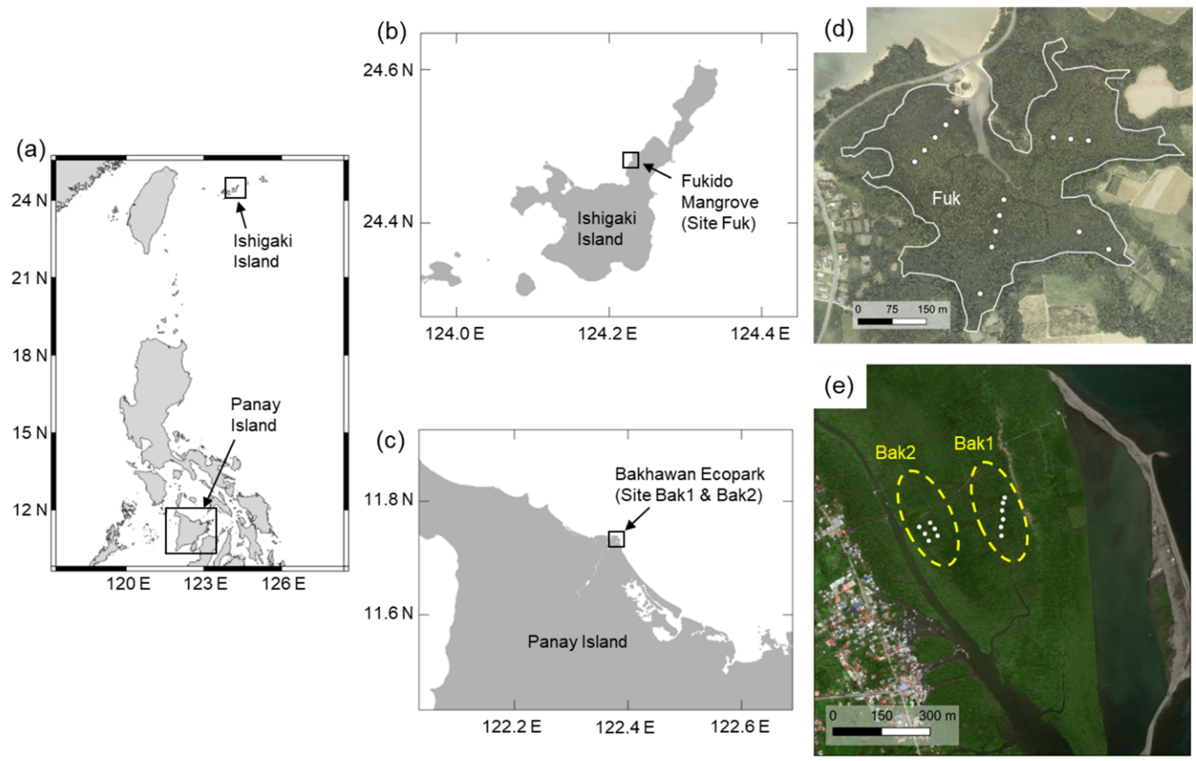

Figure S1. Map of the sites (Bak1, Bak2, and Fuk) indicated in Fig. 2. The white dots in panels "d" and "e" represent the tree census stations from which data are used in Fig. 2. In panel "e", the approximate locations of the 30-year-old (Bak1) and 17-year-old (Bak2) planted stands are also indicated. Shorelines in panel "a–c" are from the Global Self-consistent, Hierarchical, High-resolution Geography (GSHHG) database. The aerial photo in panel "d" is from Asia Air Survey Co. Ltd., Japan, and the satellite image in panel "e" is from © Google Earth.

S5. Implementation of the new model to the COAWST

We replaced the equations for drag force and turbulence introduced by Beudin et al. (2017) with the ones presented in Sections 2.1.1–2.1.2 (Eqs. (1)–(6)) in the COAWST. The *Rhizophora* root module that gives $a_{root}(z)$ from n_{tree} and $D_{stem,ave}$ using the *Rh*-root model was newly added in the COAWST (Fig. 1). Table S2 shows the grid-explicit input parameters related to this study. Parameters related to root structures are inputted to the model as universal parameters (not grid-explicit; Table S1). We introduced a new input parameter, species index (*spe*), that identifies the vegetation as *Rhizophora* species (*spe* = 1) or seagrass/marsh species (*spe* = 0). Depending on *spe*, the model interpretation of the inputted parameters varies (Table S2). If *spe* = 1, the vegetation module interacts with the *Rhizophora* root module for a_{root} (Fig. 1) to compute the drag by the roots (F_{root} in Eq. (1)) and the TKE production and dissipation of the root-generated wakes ($P_{w,root}$ and $D_{w,root}$ in Eqs. (4)–(6)). Otherwise (*spe* = 0), zero value is given to a_{root}, which vanishes all the root-related terms in Eqs. (1), (4)–(6), making them identical to the ones introduced by Beudin et al. (2017) and thus applying the cylinder drag model (however, see Sect. S2 for the modification of the equations of Beudin et al. (2017)). This means that the equations presented can be used both for *Rhizophora* mangroves and seagrasses/marshes by switching the value of *spe*.

Table S2. Grid-explicit input parameters. Symbols used in Beudin et al. (2017) are also shown. Parameters absent in the column of Beudin et al. (2017) are the ones newly added in this study. Mean tree height (H_{ave}) is only relevant for some extreme conditions when the water level becomes higher than H_{ave}.

Symbol		Unit	Interpretation by the model	
This study	Beudin et al. (2017)		Case *spe* = 1	Case *spe* = 0
spe		-	*Rhizophora* species	Seagrass/marsh
$D_{stem,ave}$	b_v	m	Mean stem diameter	Leaf width or stem diameter
n_{ree}	n_v	m^{-2}	Tree density	Leaf or stem density
H_{ave}	l_v	m	Mean tree height	Leaf or stem length

S6. Generic mangrove root model used in Xie et al. (2020)

We examined the use of the mangrove root model used in Xie et al. (2020) (termed as generic root model in the main text) as a predictor of a_{root} in Eq. (1). In Xie et al. (2020), the shape of roots was simplified to cylindrical objects with a fixed diameter and height, hence to the array of vertical cylinders. The number of roots of a tree is given by the function of stem diameter as:

$$n_{root,ind} = n_{root,max} \frac{1}{1+exp\left[f_{root}\left(\frac{D_{stem,max}}{2} - D_{stem}\right)\times 100\right]} \quad \text{(S10)}$$

where $n_{root,ind}$ is the number of roots of a tree having a stem diameter of D_{stem} (m), $n_{root,max}$ is the maximum number of roots of a tree, $f_{root} = 0.1$ is a constant describing the rate of increase of roots with D_{stem}, $D_{stem,max}$ is the maximum stem diameter (m), and the factor 100 is for the unit conversion of stem diameter from meter to centimeter. In Xie et al. (2020), the parameters are set as $n_{root,max} = 5000$, $D_{stem,max} = 1.0$ (m) for *Rhizophora* trees. In addition, Xie et al. (2020) gave the root diameter (D_{root}) and height (H_{root}) values as $D_{root} = 0.01$ m and $H_{root} = 0.15$ m, respectively.

We applied the generic root model to the field mangrove setting of Bakhawan Ecopark. We used the measured mean stem diameter $D_{stem,ave} = 0.066$ m (Table 1) for D_{stem} in Eq. (S10), then calculated the $n_{root,ind}$ with the same parameter setting as Xie et al. (2020). The a_{root}, which is used for calculating the drag by the roots in Eq. (1), is then given as:

$$a_{root} = n_{tree} n_{root,ind} D_{root} \quad \text{for } z \leq H_{root} \quad \text{(S11a)}$$

$$a_{root} = 0 \quad \text{for } z > H_{root} \quad \text{(S11b)}$$

S7. Calculation of bed shear stress in the COAWST and the choice of bed roughness value for the case of increased z_0

In the COAWST, bed shear stress is computed based on quadratic law using the velocities at the bottom computational cell as (Warner et al., 2008):

$$\tau_{bed} = \rho_w C_{bed} u^2 \quad \text{(S12)}$$

where τ_{bed} is the bed shear stress (N m^{-2}), ρ_w is the water density (kg m^{-3}), C_{bed} is the bed drag coefficient, and u is the flow velocity (m s^{-1}) computed at the bottom cell. It assumes that the flow in the bottom boundary layer has the classic vertical logarithmic profile as:

$$|u| = \frac{u_*}{\kappa} \ln\left(\frac{z_{bottom}}{z_0}\right) \quad \text{(S13)}$$

where u_* is the friction velocity, $\sqrt{\tau_{bed}}$, κ = 0.41 is the von Kármán constant, z_{bottom} is the elevation of the middle point of the bottom computational cell above the bed (m), and z_0 is the bed roughness length (m). From Eqs. (S12)–(S13), the C_{bed} is calculated using z_0 as:

$$C_{bed} = \kappa^2 \left[\ln\left(\frac{z_{bottom}}{z_0}\right)\right]^{-2} \quad \text{(S14)}$$

The value of z_0 or C_{bed} can be related to the Manning's coefficient ($n_{manning}$) considering turbulent open channel flow as follows. In an open channel flow with depth-averaged velocity U_{mean}, water depth h, and bed slope S_0, the U_{mean} can be described using the Manning's coefficient as:

$$U_{mean} = \frac{1}{n_{manning}} h^{2/3} {S_0}^{1/2} \quad \text{(S15)}$$

Assuming a steady flow where the momentum balance can be reduced to an equilibrium between the bed shear stress τ_{bed} and the gravitational (or pressure) forces driving the flow, the bed shear stress can be expressed as (Crompton et al., 2020):

$$\tau_{bed} = \rho_w g h S_0 \quad \text{(S16)}$$

where g is the gravitational acceleration (m s^{-2}). From Eq. (S15)–(S16) and assuming that the depth-averaged form of Eq. (S12), $\tau_{bed} = \rho_w C_{bed,mean} U_{mean}^2$, is valid, the Manning's coefficient can be expressed as:

$$n_{manning} = h^{1/6} \sqrt{\frac{C_{bed,mean}}{g}} \quad \text{(S17)}$$

where $C_{bed,mean}$ is the bed drag coefficient which is used for computing τ_{bed} using the U_{mean}. Also, by relating the depth-averaged form of Eq. (S14), $C_{bed,mean}$ can be expressed using z_0 as (Lenz et al., 2017):

$$C_{bed,mean} = \kappa^2 \left[\ln\left(\frac{h}{z_0}\right)\right]^{-2} \quad \text{(S18)}$$

Considering the Manning's coefficient of 0.14, which is a value typically used for approximating the drag by mangroves (e.g., Zhang et al., 2012), and a water depth of 0.5 m, based on Eqs. (S17)–(S18), the equivalent bed roughness z_0 is 0.22 m.

The application of Eqs. (12)–(14) needs the condition $z_0 < z_{bottom}$, which limits the applicable z_0 value for representing the mangrove drag depending on the water depth or thickness of the bottom cell. In the application to the field-based study, the lowest water depth for examination was around 0.15 m (Fig. 6; Table S6), where the z_{bottom} is decreased down to 0.015 m. In order to increase the applicable z_0 value in our analysis, we reduced the number of vertical layers from 5 to 3 (Table 2), which increased the minimum z_{bottom} up to 0.025 m. We then conducted the analysis using z_0 = 0.02 m as a case of increased z_0. However, this value is considered generally lower compared to the typical Manning's coefficient value of 0.14 (of which the equivalent value is z_0 = 0.22 m under the water depth 0.5 m).

Table S3. Measured flow variables in the model and field mangrove forest by Maza et al. (2017) and Yoshikai et al. (2022a), respectively, the variables controlled in the model, and target variables to reproduce for application to the respective mangrove forest.

	Model mangrove forest in Maza et al. (2017)	Field mangrove forest in Yoshikai et al. (2022a)
Measured flow variables	h, U, $u(z)$, $k(z)$	h, $\Delta\eta$, $u(z)$, U, τ_{bed}
Controlled variables in the model	h, U	h, $\Delta\eta$
Target variables to reproduce	$u(z)$, $k(z)$	$u(z)$, U, τ_{bed}

Table S4. Data from the flume experiments of Maza et al. (2017) that were used for the model validation in Figure 4. The values of geometric and flow parameters were converted from the scale in the flume to the real scale. The velocity (*u*) and turbulent kinetic energy (*k*) were taken by averaging the measurements at five lateral positions (ADV3p1–p5; see Fig. 5 of Maza et al., 2017) in the model mangrove forest where the flows were fully developed, which were taken as spatially-averaged values in the mangrove forest. HR_{max}: maximum root height, *h*: water depth, *U*: cross-sectional mean velocity, *z*: height above the bed.

Experiment #	HR_{max} (m)	h (m)	U (m s^{-1})	z (m)	u/U	k/U^2
Exp 1	2.016	3.0	0.31	0.08	0.54	0.012
				0.32	0.62	0.013
				0.56	0.66	0.015
				0.80	0.64	0.032
				1.04	0.69	0.026
				1.28	0.75	0.024
				1.52	0.84	0.053
				1.76	0.97	0.035
				2.00	1.05	0.033
				2.24	1.10	0.043
Exp 2	2.016	1.79	0.58	0.08	0.75	0.018
				0.20	0.77	0.021
				0.32	0.80	0.017
				0.44	0.84	0.016
				0.56	0.83	0.021
				0.68	0.83	0.026
				0.80	0.86	0.023
				0.92	0.85	0.023

Table S5. Data from field measurements of Yoshikai et al. (2022a) that were used for the model validation in Figure 5. Velocity (u) was obtained by averaging the measurements at four locations around the reference tree shown in Fig. S3c which was taken as spatially-averaged values in the mangrove forest.

Local time	h (m)	z (m)	u (m s^{-1})
2018/9/10 12:50	0.45	0.35	0.060
		0.30	0.064
		0.25	0.060
		0.20	0.057
		0.15	0.055
		0.10	0.044
		0.05	0.036
2018/9/10 13:40	0.21	0.18	0.096
		0.11	0.082
		0.04	0.059
2018/9/11 13:00	0.53	0.45	0.046
		0.40	0.039
		0.35	0.045
		0.30	0.044
		0.25	0.044
		0.20	0.041
		0.15	0.034
		0.10	0.028
		0.05	0.022
2018/9/11 14:00	0.28	0.23	0.085
		0.14	0.072
		0.05	0.052

Table S6. Data from field measurements of Yoshikai et al. (2022a) that were used for the model forcing and validation in Figures 6–8. The $\Delta\eta$ is the water level difference imposed across the open boundaries in the model (see Fig. S2), h is the water depth, U is the cross-sectional mean flow velocity, u_{bottom} is the spatially-averaged velocity at z = 0.05 m, and τ_{bed} is the bed shear stress.

Local time	$\Delta\eta$ (m)	h (m)	U (m s^{-1})	u_{bottom} (m s^{-1})	τ_{bed} (N m^{-2})
2018/09/10 12:50	0.0143	0.45	0.050	0.036	0.023
2018/09/10 13:10	0.0189	0.36	0.063	0.036	0.039
2018/09/10 13:20	0.0273	0.32	0.064	0.041	0.032
2018/09/10 13:40	0.0462	0.21	0.079	0.064	0.023
2018/09/10 13:50	0.0572	0.16	0.074	0.066	-
2018/09/11 13:00	0.0065	0.53	0.038	0.022	0.008
2018/09/11 13:10	0.0078	0.50	0.038	0.023	0.004
2018/09/11 13:20	0.0124	0.46	0.047	0.027	0.008
2018/09/11 13:40	0.0163	0.37	0.051	0.034	0.014
2018/09/11 13:50	0.0228	0.33	0.054	0.036	0.010

2018/09/11 14:00	0.0260	0.28	0.070	0.053	0.012
2018/09/11 14:10	0.0345	0.23	0.071	0.053	0.031
2018/09/11 14:20	0.0449	0.18	0.070	0.060	0.037
2018/09/11 14:30	0.0585	0.14	0.078	0.077	-

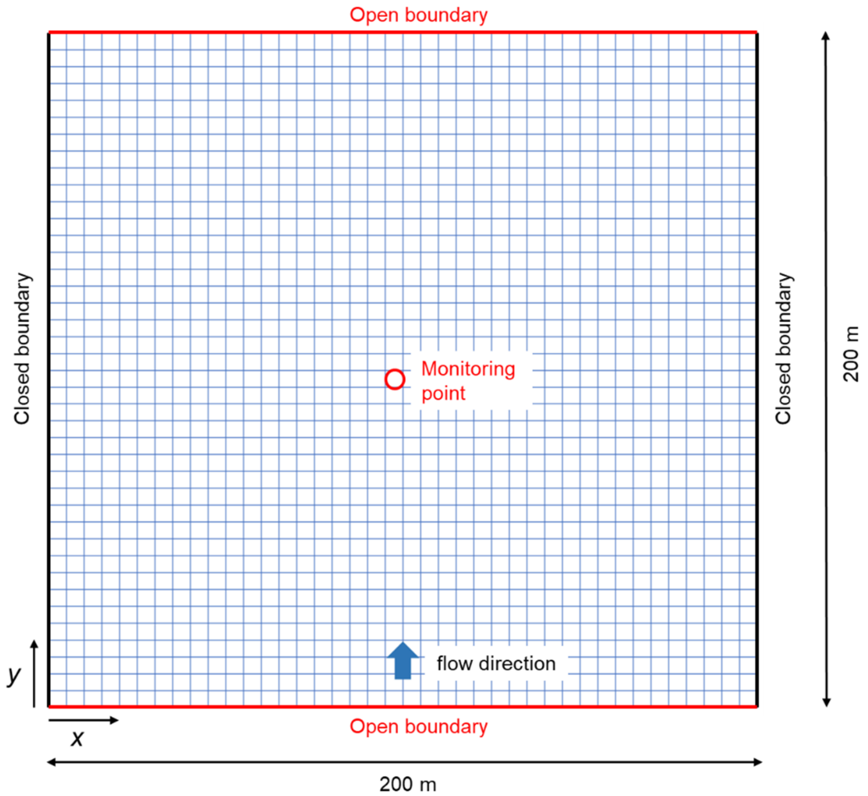

Figure S2. Model grid (40 × 40 with 5 m horizontal resolution) used for testing the model against laboratory-based and field-based studies. The red circle indicates the location of the monitoring point at which the simulated flow variables were compared with the measured data.

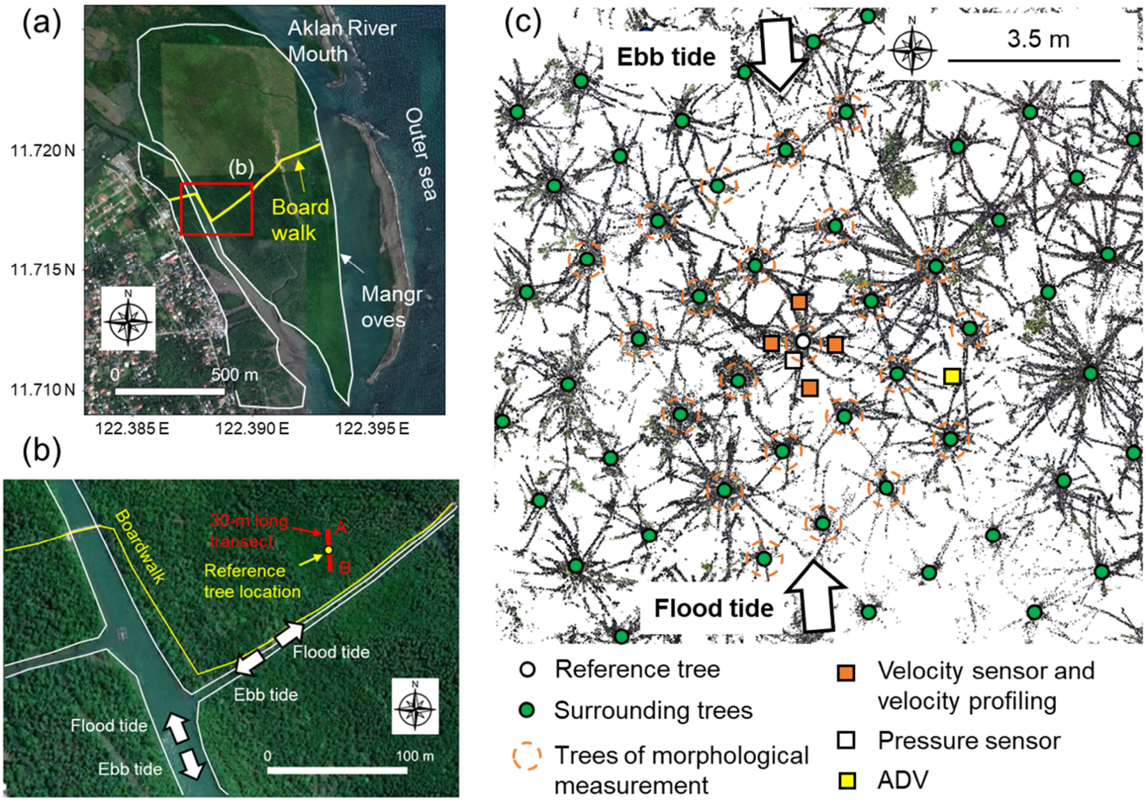

Figure S3. (a) Satellite image (© Google Earth) of the study site of Yoshikai et al. (2022a) – Bakhawan Ecopark (red box indicates the area of panel "b"), (b) locations of transect A–B across which the water level gradient was measured together with the hydrodynamic parameters around the reference tree (the satellite image is from © Google Earth), (c) top view of LiDAR point clouds around the reference tree with information on the locations of trees whose morphological structures were measured, where velocity profiling was conducted, and where sensors were deployed (velocity sensor: electromagnetic velocity meter deployed near the bottom; ADV: Acoustic Doppler Velocimeter deployed to estimate the bed shear stress). It has been shown in Yoshikai et al. (2022a) that the average of the velocity measured at the four locations represents well the spatially-averaged values. The point clouds shown were cropped at heights between 0.1–1.7 m for better visualization of the root systems. Figures are modified from Yoshikai et al. (2022a).

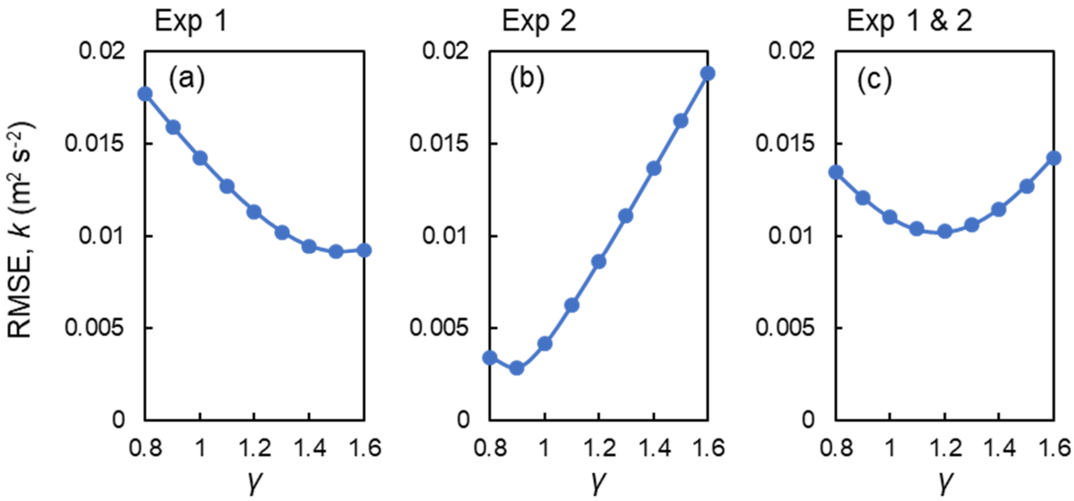

Figure S4. Root mean square error (RMSE) of modeled turbulent kinetic energy (*k*) against the measured data in (a) Exp 1, (b) Exp2, and (c) both Exp 1 and 2 of the flume experiment, by varying the value of scale coefficient (*γ*), for which the computation of the predicted value at the height of the measurement point was obtained by the interpolation of *k* computed at adjacent vertical layers.

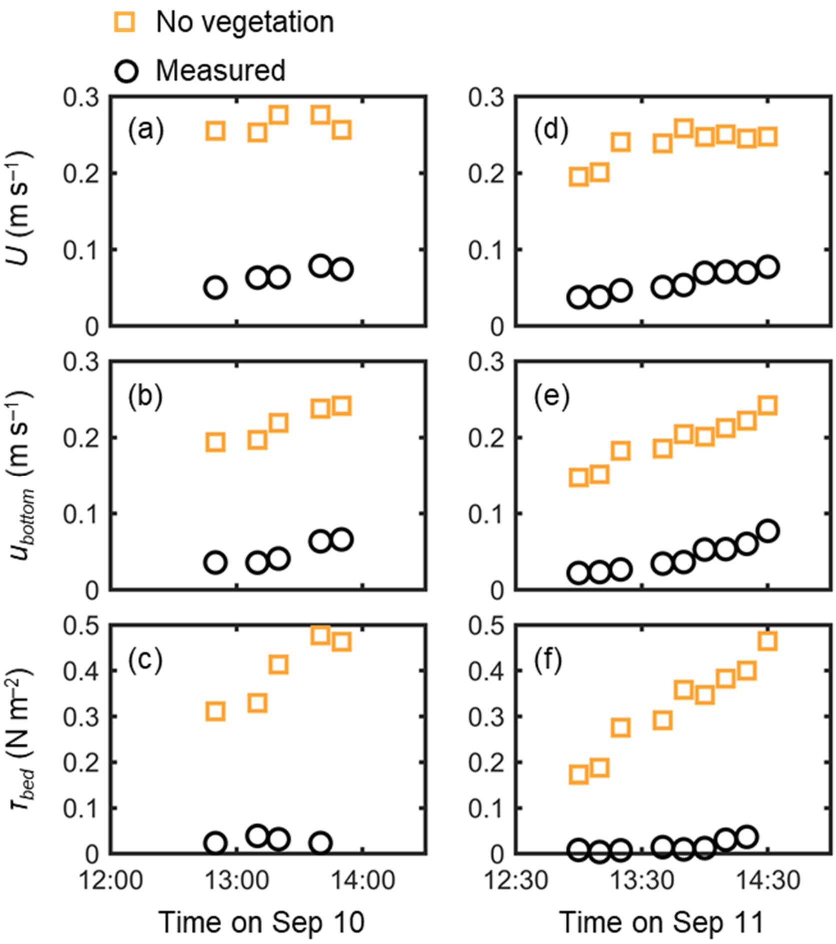

Figure S5. Time-series of measured and predicted (a, d) cross-sectional mean velocity (U), (b, e) (spatially averaged) velocity at z = 0.05 m, and (c, f) bed shear stress (τ_{bed}) during the two-days measurement in Bakhawan Ecopark. The measured values are from Yoshikai et al. (2022a) and the predicted values are obtained through the COAWST without imposing vegetation drag (no vegetation).

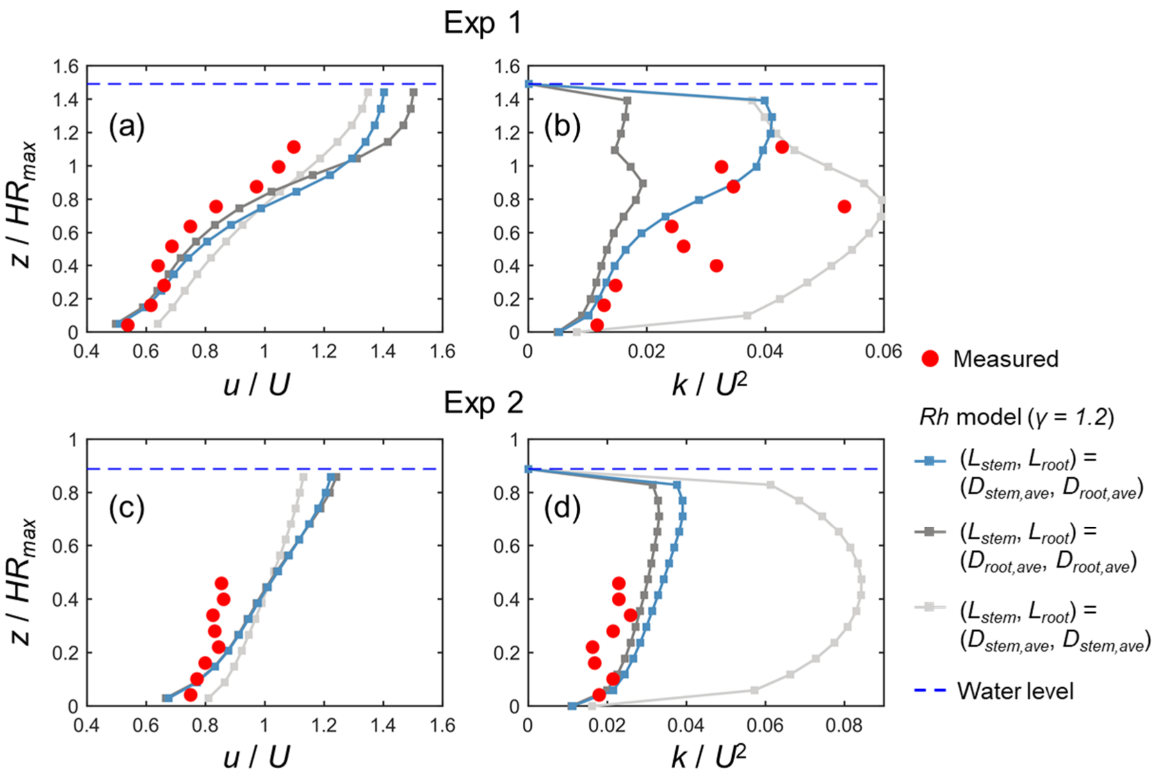

Figure S6. Comparison of the vertical profiles of (temporally and spatially averaged) velocity (u) and turbulent kinetic energy (k) normalized by the cross-sectional mean velocity (U) measured by Maza et al. (2017) and predicted by the COAWST using the Rh model with different length-scales of stem- and root-generated wakes (L_{stem} and L_{root}, respectively) defined – blue markers: L_{stem} and L_{root} set to the stem diameter ($D_{stem,ave}$) and root diameter ($D_{root,ave}$), respectively; dark-gray markers: L_{stem} and L_{root} both set to $D_{root,ave}$; light-gray markers: L_{stem} and L_{root} both set to $D_{stem,ave}$. The scale coefficient (γ) was set to 1.2 for all the cases.

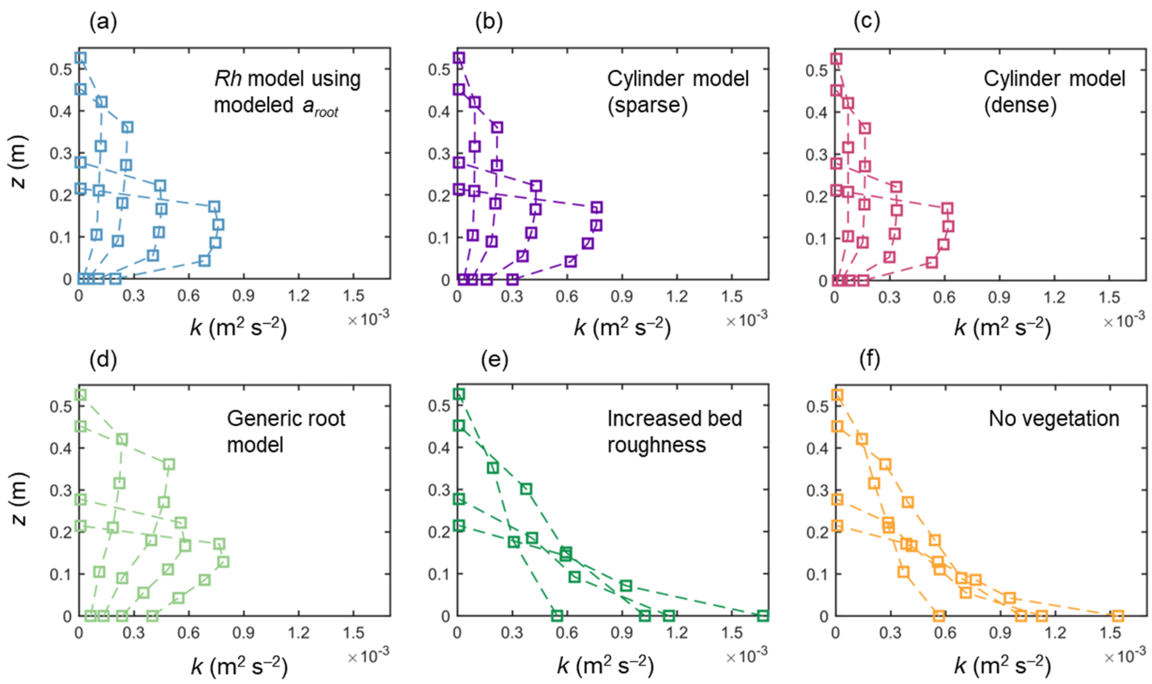

Figure S7. Vertical profiles of turbulent kinetic energy (k) predicted by the COAWST employing (a) *Rh* model using modeled root projected area density profile (a_{root}), (b) cylinder model with sparse and (c) dense arrays, (d) generic root model, (e) increased bed roughness as an approximation of vegetation drag, and (f) without imposing vegetation drag (no vegetation) for some tidal phases corresponding to the ones shown in Fig. 5.

References

Baptist, M. J., Babovic, V., Rodríguez Uthurburu, J., Keijzer, M., Uittenbogaard, R. E., Mynett, A., and Verwey, A.: On inducing equations for vegetation resistance. Journal of Hydraulic Research, 45(4), 435–450. https://doi.org/10.1080/00221686.2007.9521778, 2007.

Beudin, A., Kalra, T. S., Ganju, N. K., and Warner, J. C.: Development of a coupled wave-flow-vegetation interaction model. Computers & Geosciences, 100, 76–86. https://doi.org/10.1016/j.cageo.2016.12.010, 2017.

Crompton, O., Katul, G. G., and Thompson, S.: Resistance formulations in shallow overland flow along a hillslope covered with patchy vegetation. Water Resources Research, 56, e2020WR027194. https://doi.org/10.1029/2020WR027194, 2020.

Defina, A. and Bixio, A. C.: Mean flow and turbulence in vegetated open channel flow. Water Resources Research, 41(7). https://doi.org/10.1029/2004WR003475, 2005.

King, A. T., Tinoco, R. O., and Cowen, E. A.: A k–ε turbulence model based on the scales of vertical shear and stem wakes valid for emergent and submerged vegetated flows. Journal of Fluid Mechanics, 701, 1–39. https://doi.org/10.1017/jfm.2012.113, 2012.

Lentz, S. J., Davis, K. A., Churchill, J. H., and DeCarlo, T. M.: Coral reef drag coefficients-water depth dependence. Journal of Physical Oceanography, 47(5), 1061–1075. https://doi.org/10.1175/jpo-d-16-0248.1, 2017.

Liu, Z., Chen, Y., Wu, Y., Wang, W., and Li, L.: Simulation of exchange flow between open water and floating vegetation using a modified RNG k-ε turbulence model. Environ Fluid Mech 17, 355–372. https://doi.org/10.1007/s10652-016-9489-5, 2017.

López, F. and García, M. H.: Mean flow and turbulence structure of open-channel flow through non-emergent vegetation. Journal of Hydraulic Engineering, 127(5), 392–402. https://doi.org/10.1061/(ASCE)0733-9429(2001)127:5(392), 2001.

Nepf, H. M.: Flow and transport in regions with aquatic vegetation. Annual review of fluid mechanics, 44, 123–142. https://doi.org/10.1146/annurev-fluid-120710-101048, 2012.

Suwa, R., Rollon, R., Sharma, S., Yoshikai, M., Albano, G. M. G., Ono, K., Adi, N. S., Ati, R. N. A., Kusumaningtyas, M. A., Kepel, T. L., Maliao, R. J., Primavera-Tirol, Y. H., Blanco, A. C., and Nadaoka, K.: Mangrove biomass estimation using canopy height and wood density in the South East and East Asian regions. Estur. Coast. Shelf S., 248, 106937, 2021.

Tanino, Y. and Nepf, H. M.: Lateral dispersion in random cylinder arrays at high Reynolds number. Journal of Fluid Mechanics, 600, 339–371. https://doi.org/10.1017/S0022112008000505, 2008.

Warner, J. C., Sherwood, C. R., Signell, R. P., Harris, C. K., and Arango, H. G.: Development of a three-dimensional, regional, coupled wave, current, and sediment-transport model. Computers & geosciences, 34(10), 1284–1306. https://doi.org/10.1016/j.cageo.2008.02.012, 2008.

Xie, D., Schwarz, C., Brückner, M. Z., Kleinhans, M. G., Urrego, D. H., Zhou, Z., and Van Maanen, B.: Mangrove diversity loss under sea-level rise triggered by bio-morphodynamic feedbacks and anthropogenic pressures. Environmental Research Letters, 15(11), 114033. https://doi.org/10.1088/1748-9326/abc122, 2020.

Yoshikai, M., Nakamura, T., Suwa, R., Argamosa, R., Okamoto, T., Rollon, R., Basina, R., Primavera-Tirol, Y. H., Blanco, A. C., Adi, N. S., and Nadaoka, K.: Scaling relations and substrate conditions controlling the complexity of Rhizophora prop root system. Estur. Coast. Shelf S., 248, 107014, 2021.

Yoshikai, M., Nakamura, T., Bautista, D. M., Herrera, E. C., Baloloy, A., Suwa, R., Basina, R., Primavera-Tirol, Y. H., Blanco, A.C., and Nadaoka, K.: Field measurement and prediction of drag in a planted Rhizophora mangrove forest. Journal of Geophysical Research: Oceans, 127, e2021JC018320. https://doi.org/10.1029/2021JC018320, 2022a.

Yoshikai, M., Nakamura, T., Suwa, R., Sharma, S., Rollon, R., Yasuoka, J., Egawa, R., and Nadaoka, K.: Predicting mangrove forest dynamics across a soil salinity gradient using an individual-based vegetation model linked with plant hydraulics. Biogeosciences, 19(6), 1813–1832. https://doi.org/10.5194/bg-19-1813-2022, 2022b.

Zhang, K., Liu, H., Li, Y., Xu, H., Shen, J., Rhome, J., and Smith III, T. J.: The role of mangroves in attenuating storm surges. Estuarine, Coastal and Shelf Science, 102, 11–23. https://doi.org/10.1016/j.ecss.2012.02.021, 2012.